



Computer-Assisted Histopathological Calculation Analysis of the Sciatic Nerve of Diabetic Neuropathy Rat Model

Indah Tri Lestari ^{1,2*}  

Kusnandar Anggadiredja ³   

Afrillia Nuryanti Garmana ⁴  

Sevi Nurafni ⁵  

¹ Doctoral Program of Pharmacy, [Institut Teknologi Bandung](#), Bandung, West Java, Indonesia

² Department of Pharmacy, [Universitas Darussalam Gontor](#), Ponorogo, East Java, Indonesia

³ Department of Pharmacology and Clinical Pharmacy, [Institut Teknologi Bandung](#), Bandung, West Java, Indonesia

⁴ Department of Pharmacy, [Institut Teknologi Bandung](#), Bandung, West Java, Indonesia

⁵ Department of Data Science, [Universitas Koperasi Indonesia](#), Sumedang, West Java, Indonesia

*email: indahtrilestari94@gmail.com; phone: +6288809456318

Keywords:

Gaussian adaptive threshold
Histopathology digitization
ImageJ plugin
Sciatic nerve

Abstract

Histopathology is the science that studies the signs of disease by studying the structural and functional changes that occur in cells using certain types of dyes such as hematoxylin and eosin (H&E). Traditionally histopathological testing is carried out using semi-quantitative methods. A more advanced method is done by taking photos digitally, and then digital photos are quantified with the help of software such as ImageJ using plugin tools. Recent advances in digital pathology require the development of more efficient computerized image analysis such as the Gaussian adaptive threshold method. This research aims to compare the calculation results of computer-assisted digitalization of histopathology using the ImageJ plugin manual method with automatic calculations using Gaussian adaptive threshold to quantify the amount of sciatic nerve cell damage in the Diabetic peripheral neuropathy (DPN) rat model. In this study, two image analysis methods were used to test their ability to measure the amount of cell damage in the sciatic nerve of normal rats using a model of diabetic neuropathy. The first method uses the ImageJ plugin manual. The second method is the Gaussian adaptive threshold method. The ImageJ plugin manual method obtained a cell abnormality value of 213 cells. Meanwhile, with the Gaussian adaptive threshold method, a value of 204 cells was obtained. The calculation results of the two methods show an insignificant difference between the methods $p > 0.05$. This study presents a computerized morphometric image analysis method with the potential for pathology digitalization applications.

Received: January 15th, 2024

1st Revised: May 21st, 2024

Accepted: May 22nd, 2024

Published: May 30th, 2024



© 2024 Indah Tri Lestari, Kusnandar Anggadiredja, Afrillia Nuryanti Garmana, Sevi Nurafni. Published by [Institute for Research and Community Services Universitas Muhammadiyah Palangkaraya](#). This is an Open Access article under the CC-BY-SA License (<http://creativecommons.org/licenses/by-sa/4.0/>). DOI: <https://doi.org/10.33084/bjop.v7i2.6590>

INTRODUCTION

Histopathology is the science that studies the signs of disease by studying the structural and functional changes that occur in cells and tissues. Visualization of differences in tissue components under a microscope is carried out by processing tissue biopsies or specimens and mounting them on glass slides, then the tissue is stained in such a way as to provide color contrast between the cells. Several types of dyes such as hematoxylin-eosin, immunohistochemistry, or immunofluorescence labeling have been widely used¹.

Hematoxylin and eosin (H&E) staining is the most commonly used light microscope staining method in histopathology laboratories and has been used by pathologists for over one hundred years. The H&E staining allows increasing contrast and distinguishing between nuclei and cytoplasm in tissues. Hematoxylin colors the cell nucleus blue, formed from aluminum ions and oxidized hematoxylin, while eosin colors the cytoplasm and connective tissue pink. Due to H&E's long history, established methods, and a large amount of data and publications, there is a strong belief among many pathologists that the practice of H&E will continue for the next 50 years². Traditionally, histopathological testing is carried out by a

pathologist using the eye to directly observe whether there are damages, differences, or cancer cells in a tissue sample after staining under a microscope using the semi-cutification method. This method takes time and effort. In addition, traditional detection methods are subjective and lack quantitative feature parameters as a reference, resulting in different recognition accuracies³.

A more advanced method involves taking photos digitally with the help of software such as ImageJ and calculating manually using plug-in tools. Cell Counter Plug-in from the ImageJ platform (<https://imagej.net/ij/index.html>) was used to precisely count cell nuclei. ImageJ is a Java-based public domain image analysis program. ImageJ has become the image processing tool in many laboratories. However, counting nuclei one by one is laborious and time-consuming. Therefore, it becomes less effective in laboratories with a large number of cases for diagnosis, so automatic calculations of cellular nuclei using software began to be developed⁴. Therefore, efficient quantitative, stable, and accurate analysis detection, as well as cell image identification are the focus of many research works³.

As technology develops, computer-aided disease diagnosis (CAD) plays a very important role and has become a major research subject in histopathological imaging and diagnostics. Computer-assisted histopathological studies have been performed for various breast cancer detection and assessment applications^{4,6}, colon^{7,8}, lung⁹, prostate¹⁰, skin^{11,12}, and other cancers. However, histopathological detection of other diseases is still very limited. One of the diseases that may be observed with computer-assisted histopathological studies is damage to the sciatic nerve tissue in diabetic neuropathy. Diabetic neuropathy is a rapidly growing pathology and should be of global concern. In most cases, diabetic neuropathy begins as a small fiber neuropathy affected by lower serum glucose levels and blood flow¹³. Several human and animal studies have shown that hyperglycemia-related damage to unmyelinated C fibers, small myelinated A δ fibers, and large myelinated A β fibers contribute to the development of diabetic peripheral neuropathy (DPN)¹⁴.

Over the past few years, studies in animal models have begun to yield important insights into the mechanisms of pain in DPN. The streptozotocin (STZ)-induced rat model is the most widely used experimental model in diabetes models similar to humans. Induction of inflammation has been associated with microvascular tissue and nerve damage in human diabetes and rodent models of diabetes. The observed morphological damage could provoke functional deficits of the sciatic nerve in untreated diabetic rats. The presence of abnormal fibers in the sciatic nerve with axonal degeneration and myelin damage is one of the symptoms of streptozotocin-induced diabetes in rats¹⁵. The large number of abnormal cells in the sciatic nerve can indicate the severity of diabetic neuropathy. Therefore, it is hoped that quantification of abnormal cells can be the basis for diagnosing the severity of diabetic neuropathy in the future. Recent advances in digital pathology have required the development of quantitative computerized image analysis and automated algorithms to assist pathologists interpreting large numbers of histopathological digital images¹⁶.

In this study, a comparative method of computer-assisted histopathological digital image analysis was carried out on the sciatic nerve from an animal model of diabetic neuropathy using manual calculations using the ImageJ plugin and Gaussian adaptive threshold to quantify observable cell abnormalities. This histological assessment will provide important insight into the phenotypic properties of the tissue microenvironment. This is in line with the development of pharmaceutical research which often relies on visual assessment of tissue morphology, either for characterization of *in vivo* experiments, pharmacodynamics, and mechanisms of action of drugs, as well as toxicological assessments or as criteria for clinical trials. Automatic computational analysis of histopathology data is expected to speed up tissue analysis work and provide more objective quantitation with rapidly developing technology, thereby increasing the effectiveness and performance of researchers.

MATERIALS AND METHODS

Materials

The materials used in this study included a sciatic pain rat model, CO₂ gas, 10% formalin, paraffin wax blocks, 95% ethanol, eosin, hematoxylin, xylene, and distilled water. The instrument and software used included a microscope, ImageJ, and Gaussian analysis program.

Methods

The H&E staining and image digitization

Diabetic peripheral neuropathy rats were euthanized by placing them in a closed container with a flow of CO₂ gas. Sciatic nerve tissue was taken and fixed in 10% buffered formalin. After fixation, the tissue was dehydrated in gradient ethanol (70-95%). The tissue was then cleaned using xylene. Tissue was embedded in paraffin wax blocks for sectioning and sectioned to a thickness of 5 µm using a microtome. Tissue samples were placed on microscope slides and deparaffinized using xylene (100%), then rehydrated with absolute ethanol, gradient ethanol, and finally distilled water. The slides were then washed using distilled water and soaked in hematoxylin for 3-8 minutes. The slides were then cleaned with running water for 20 minutes and then rehydrated with ethanol 70-95%. The slides were then stained with eosin for 30 seconds, rinsed again with gradient ethanol immediately, and finally dried. Xylene was added to clear the tissue. The slide was then covered with a coverslip. The slides were analyzed microscopically and photographs were taken under a microscope at 4x and 10x magnification¹⁷. This study has been approved by the Animal Ethic Committee of Institut Teknologi Bandung with approved ID 08/KEPHP-ITB/3-2022.

Manual analysis with ImageJ plugin

Cell counting was performed using ImageJ software (<https://imagej.net/ij/download.html>) according to the instructions¹⁸. To count the cells, ImageJ was first installed. Then, the Cell Counter plugin was accessed by navigating to Plugins → Analyze → Cell Counter. This plugin is compatible with single grayscale, single-color, or multicolor images. Grayscale images were identified by "8-bit" or "16-bit" at the top, while color images were labeled "RGB". Cells were counted by clicking on them in the image. Each click added a colored box around the cell and updated the count. If an object was mistakenly included, it could be removed using Edit → Undo (limited to one undo per action). After finishing the counting process, the total cell count was obtained by clicking Analyze → Measurements in the Results window. Results could be filtered, copied and pasted, or saved as an Excel .xls spreadsheet. Saving tagged images required using the Print Screen key and saving the capture as a .tif or .jpg file.

Analysis with Gaussian adaptive threshold

The first image (Image 0) was created to show the original image. The program first read the image named "Image.jpeg" and saved it in the variable 'im'. The image was then displayed. Next, the program converted the image in 'im' to grayscale and stored it in the variable 'Gray1'. The grayscale image was then smoothed using a Gaussian filter with a kernel of (5,5) and stored in the variable 'grey'. Variables were then configured for adaptive threshold processing: -maxValue = 255, -adaptiveMethod = cv2.ADAPTIVE_THRESH_GAUSSIAN_C, -thresholdType = cv2.THRESH_BINARY, -blockSize = 3, -C = 2. The adaptive threshold process was carried out on the 'grey' image using the configured variables. The results of the process were stored in the variable 'im_threshold'. The connected objects in the image 'im_threshold' were calculated using the 'label' function in the SciPy library. The image labels were stored in the variable 'label_array'. The number of connected objects in the variable 'particle_count' was displayed in a comment line.

Data analysis

Analysis data was collected from three different areas of the image and then averaged to obtain the results. The resulting data was analyzed using paired T-test statistics, with a p-value of <0.05.

RESULTS AND DISCUSSION

Visualizing and annotating histopathology images is crucial for pharmaceutical research and clinical trials¹⁹. This study employed an automatic testing procedure with the Gaussian adaptive method to quantify histopathological features. The results showed no significant difference between the automatic method and manual calculations. Diabetic neuropathy involves oxidative damage that alters nerve structure. These changes, including axonal degeneration, segmental demyelination, and Schwann cell apoptosis, lead to damage or loss of myelin and unmyelinated fibers in patients. These histopathological changes manifest as distinct image features and colors between the normal and DPN groups, forming the

basis for the Gaussian method calculations. The study utilized a neuropathic diabetic pain model with nerve injury to induce hyperalgesia and allodynia in rodents, mimicking aspects of human neuropathic pain.

In histopathological testing, the first step involves preparing tissue slides. To better visualize specific structures within the tissue, such as the nucleus and cytoplasm, staining is necessary. The (H&E) staining is the most common method used for histopathological examination of the sciatic nerve. Hematoxylin selectively binds to DNA, staining the nucleus blue or purple, while eosin stains other cellular components pink, allowing for clear differentiation of various structures²⁰.

Following histopathological staining, the slides are examined under a microscope and digitized using a camera. Representative areas were captured as digital images using a smartphone camera. The images were taken at a magnification of 40x objective lens and 10x eyepiece lens. Since magnification affects the level of detail visible, adjusting the image threshold might be necessary for optimal analysis. Three images were chosen for cell analysis. Due to their large file size, captured RGB images are typically compressed using JPEG or JPEG 2000 formats²¹.

Several factors can introduce challenges in creating optimal image designs for automated analysis of histopathology slides. These challenges arise from variations that can occur during tissue preparation, staining, and slide digitization²². Improper fixation, for example, can alter tissue morphology, leading to inaccurate results from image analysis software. Differences in protocols and the appearance of staining reagents can vary considerably between laboratories. Even within a single lab, staining results may differ due to pre-analytical factors like fixation delays or incompatible staining conditions. Finally, variations in slide scanners' optics, photodetectors, and light sources can contribute to display inconsistencies. The histopathological findings in this study reveal a loss of regularity in the nerve fibers. This is attributed to nerve fiber degeneration, impaired myelin density, Schwann cell degeneration, and endometrial edema, as shown in **Figure 1**.

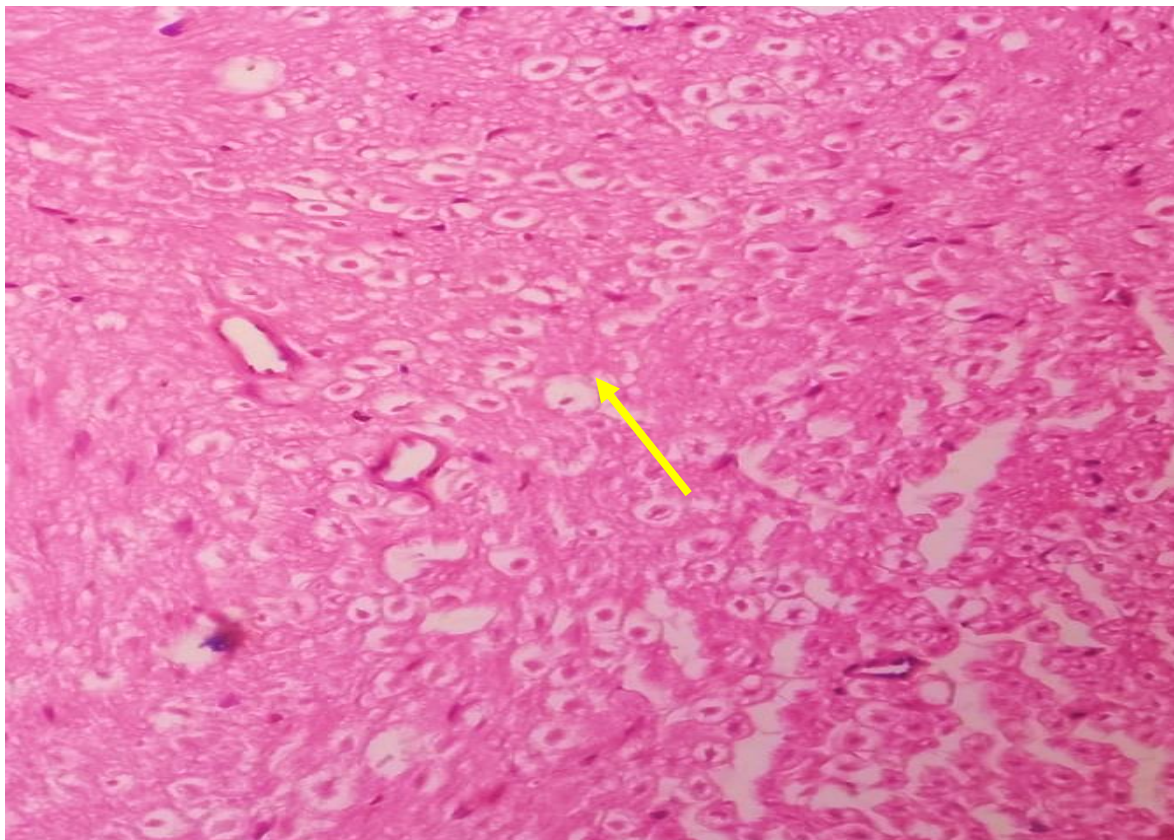


Figure 1. Histopathology results of the sciatic nerve in diabetic rat neuropathology, the yellow arrow indicates damaged cells included in the calculation.

ImageJ software, with its plugin feature, was used to analyze the digitized images. Plugins are functionalities available on all ImageJ versions, including the original (version 1), ImageJ2, and Fiji. These plugins appear in the plugin menu (or a submenu) upon starting ImageJ. They enable various tasks beyond cell damage analysis, such as image rendering, user interface extensions, processing single-image microscopy data, and result analysis. This even includes finding and adjusting image points for reconstruction²³. The results of image analysis using the ImageJ plugin can be seen in **Figure 2**.

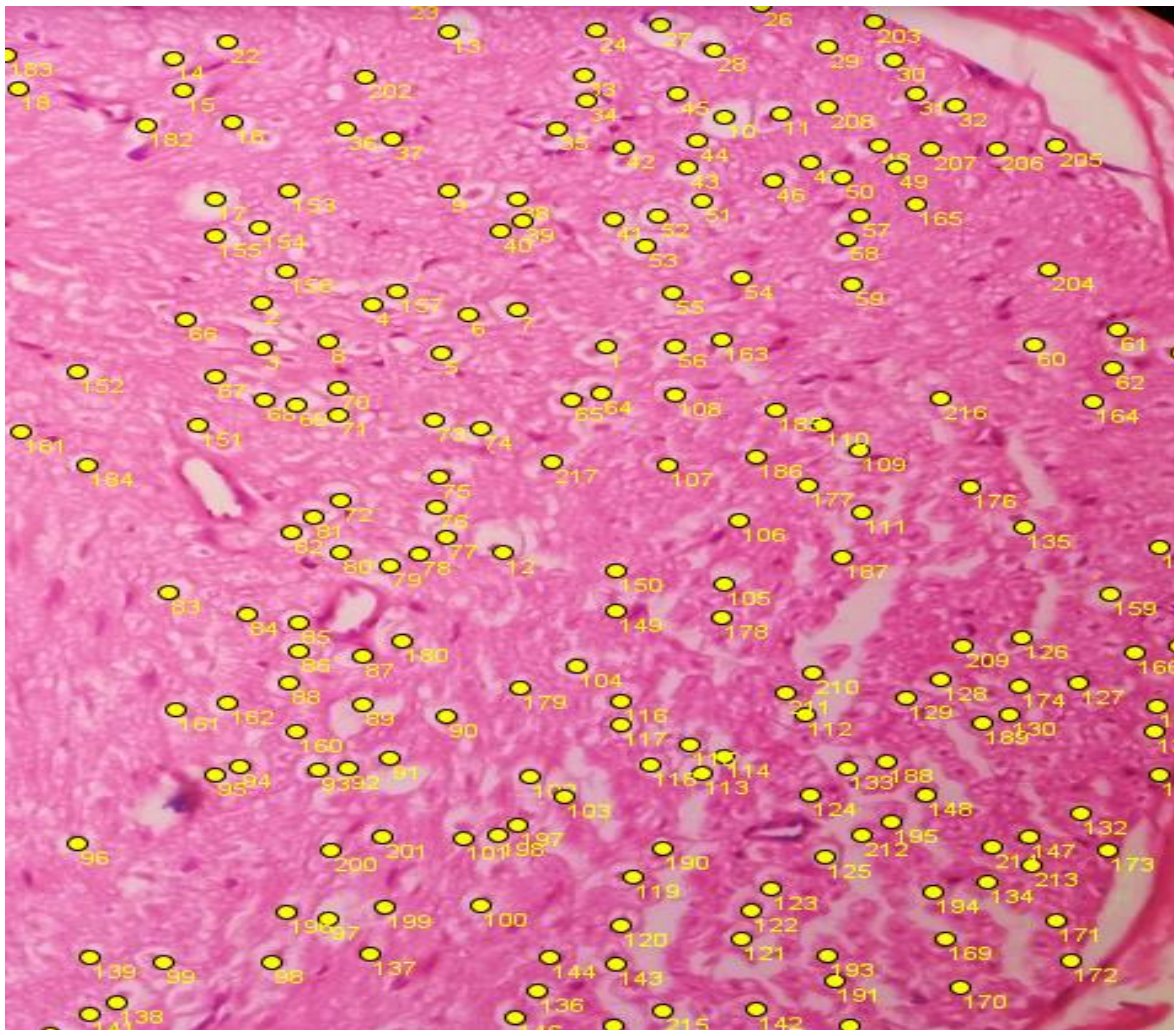


Figure 2. Presentation of manual calculations using ImageJ, yellow dots indicate counted cells.

For comparison purposes, the digitized images were also analyzed using the Gaussian adaptive thresholding method. This method divides the image into smaller regions, and calculates a specific threshold value for each region. This approach helps retain more information compared to simpler thresholding techniques. The threshold values are determined using a Gaussian function. Adaptive thresholding is particularly suitable for images with relatively uniform intensity levels²⁴.

The Gaussian adaptive thresholding method involves several steps. First, the color microscope image is converted to grayscale. Then, adaptive threshold segmentation is applied to identify background pixels. This technique classifies pixels based on their intensity: pixels brighter than a certain threshold are considered background, while darker pixels are considered foreground objects. The key factor in segmentation is the threshold value. In this method, the threshold for each pixel is calculated adaptively as the average intensity of its surrounding pixels within a 3×3 square region. Finally, binary segmentation creates a new image where each pixel is assigned a value of 0 (background) or 1 (object). Binarization essentially converts grayscale images into black and white (foreground and background). Gaussian adaptive threshold is particularly useful for images with uneven lighting or variations in pixel intensity²⁵.

The Gaussian adaptive thresholding method uses an odd-sized block to analyze the image. This allows each block to have a unique threshold value that adapts to local variations in pixel intensity. A constant value (C) is then subtracted from the average intensity within each block to achieve the desired segmentation²⁶. This technique is particularly effective at isolating individual nuclei, even those with faint or blurred boundaries, from the surrounding tissue²⁷. The results of this image processing step are shown in **Figure 3**.

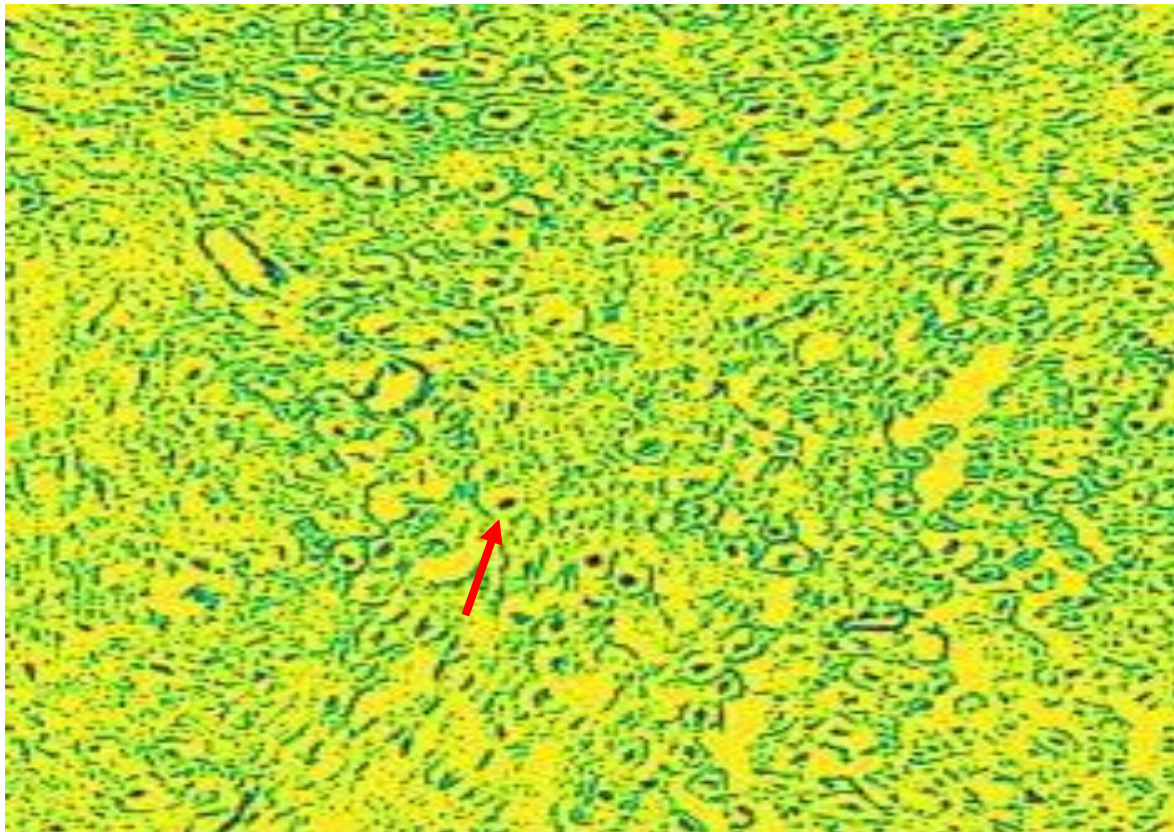


Figure 3. Presentation of calculation results with Gaussian adaptive threshold after normalization. Red arrows show examples of counted cells. In Gaussian the value is shown automatically.

To obtain quantitative data, measurements were taken from three distinct regions of the sciatic nerve in a single slide. This approach ensures a comprehensive analysis of the sample. The measurements were then averaged to produce mean values, which are presented in a graph in **Figure 4**. This visual representation facilitates data interpretation and comparison. **Figure 4** shows that the average cell count obtained using ImageJ (213.00 ± 19.31 cells) is higher compared to the average obtained using Gaussian adaptive thresholding (204.67 ± 5.03 cells). This difference can be attributed to the underlying calculation principles. Manual analysis with ImageJ involves manually counting damaged nerve cells one by one. In contrast, Gaussian adaptive thresholding automates the process. By selecting an appropriate threshold, it converts the histopathology image into a binary image, preserving only essential information about the size and shape of the nuclear regions. This simplification reduces image complexity and facilitates feature extraction and classification²⁸. Our findings align with previous study comparing manual and automated cell counting methods, which showed no significant differences in the average cell counts. The observed difference in standard deviation in this study might be due to a sample size of less than 100 slides, which is considered insufficient for statistically robust estimation of standard deviation²⁹.

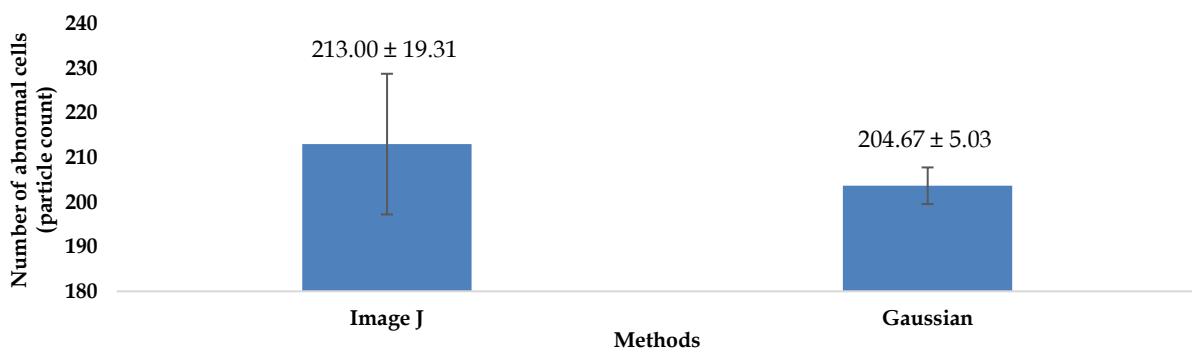


Figure 4. Comparison of abnormal cell calculations with ImageJ and Gaussian.

This study explores the use of Gaussian adaptive thresholding for cell analysis in histopathology images. However, the method has limitations. Closely spaced cell nuclei might be misidentified as a single object, and inflammatory cells with similar color intensity may also be misinterpreted. Additionally, variations in background color intensity can affect results. Manual cell counting using software like ImageJ offers an alternative approach, but it suffers from limitations such as time consumption, high workload, and potential subjectivity. The digitization of biological data opens doors for computer-aided diagnosis³⁰. While this study has not yet evaluated the accuracy of machine learning methods for this purpose, and the sample size remains relatively small, the precise calculation results obtained here suggest promise for developing a robust analytical method in the future.

The ever-growing use of computers, coupled with the development of advanced image analysis algorithms, has fueled the development of computer-assisted approaches for analyzing biomedical data. Manual interpretation of tissue slides is a laborious, expensive process prone to human error and inconsistency. Automated image analysis offers a faster, more reproducible method for generating additional insights, aiding pathologists in reaching accurate diagnoses. However, challenges remain in computer-assisted diagnosis. One hurdle is achieving the necessary accuracy and speed to provide truly useful results, particularly when dealing with the large datasets generated by digital histology samples. Additionally, ensuring accessibility of these methods to the entire pathology community is another crucial hurdle to overcome³¹.

CONCLUSION

The calculation results of the two methods show no significant differences between the methods. The test results show that the computerized morphometric image analysis method has the potential to be applied in the digitalization of pathology because it can provide an image-based environment for managing and interpreting information generated from images on glass slides into quantitative data. This digitalization also offers substantial results in improving the safety of pharmaceutical drugs in toxicology testing, preclinical pathology, and clinical trials.

ACKNOWLEDGMENT

This work was funded by the Centre for Education Services (*Pusat Layanan Pendidikan*) under the Ministry of Education, Culture, Research and Technology of the Republic of Indonesia. Research Funding scheme from the Indonesian Education Scholarship (*Beasiswa Pendidikan Indonesia; BPI*) and the Indonesia Endowment Funds for Education (*Lembaga Pengelola Dana Pendidikan; LPDP*) [Grant number: 202101121414].

AUTHORS' CONTRIBUTION

Conceptualization: Indah Tri Lestari

Data curation: Indah Tri Lestari, Sevi Nurafni

Formal analysis: Indah Tri Lestari, Sevi Nurafni

Funding acquisition: Indah Tri Lestari

Investigation: Indah Tri Lestari, Sevi Nurafni

Methodology: Sevi Nurafni

Project administration: Kusnandar Anggadiredja, Afrillia Nuryanti Garmana

Resources: Indah Tri Lestari, Sevi Nurafni

Software: Indah Tri Lestari, Sevi Nurafni

Supervision: Kusnandar Anggadiredja, Afrillia Nuryanti Garmana

Validation: Sevi Nurafni

Visualization: Indah Tri Lestari

Writing - original draft: Indah Tri Lestari

Writing - review & editing: Kusnandar Anggadiredja, Afrillia Nuryanti Garmana

DATA AVAILABILITY

None.

CONFLICT OF INTEREST

The authors declare there is no conflict of interest.

REFERENCES

1. Jimenez-del-toro O, Otálora S, Andersson M, Eurén K, Hedlund M, Rousson M, et al. Chapter 10 - Analysis of Histopathology Images: From Traditional Machine Learning to Deep Learning. In: Depeursinge A, Al-Kadi OS, Mitchell JR, editors. *Biomedical Texture Analysis: Fundamentals, Tools and Challenges*. Cambridge (MA): Academic Press; 2018. p. 281–314. DOI: [10.1016/B978-0-12-812133-7.00010-7](https://doi.org/10.1016/B978-0-12-812133-7.00010-7)
2. Gurcan MN, Boucheron LE, Can A, Madabhushi A, Rajpoot NM, Yener B. Histopathological image analysis: a review. *IEEE Rev Biomed Eng*. 2009;2:147–71. DOI: [10.1109/rbme.2009.2034865](https://doi.org/10.1109/rbme.2009.2034865); PMID: [PMC2910932](https://pubmed.ncbi.nlm.nih.gov/20671804/); PMID: 20671804
3. He W, Liu T, Han Y, Ming W, Du J, Liu Y, et al. A review: The detection of cancer cells in histopathology based on machine vision. *Comput Biol Med*. 2022;146:105636. DOI: [10.1016/j.compbimed.2022.105636](https://doi.org/10.1016/j.compbimed.2022.105636); PMID: [35751182](https://pubmed.ncbi.nlm.nih.gov/35751182/)
4. Fulawka L, Halon A. Proliferation Index Evaluation in Breast Cancer Using ImageJ and ImmunoRatio Applications. *Anticancer Res*. 2016;36(8):3965–72. PMID: [27466501](https://pubmed.ncbi.nlm.nih.gov/27466501/)
5. da Silva LG, da Silva Monteiro WRS, de Aguiar Moreira TM, Rabelo MAE, de Assis EACP, de Souza GT. Fractal dimension analysis as an easy computational approach to improve breast cancer histopathological diagnosis. *Appl Microsc*. 2021;51(1):6. DOI: [10.1186/s42649-021-00055-w](https://doi.org/10.1186/s42649-021-00055-w); PMID: [PMC8087740](https://pubmed.ncbi.nlm.nih.gov/33929635/); PMID: 33929635
6. Burrai GP, Gabrieli A, Polinas M, Murgia C, Becchere MP, Demontis P, et al. Canine Mammary Tumor Histopathological Image Classification via Computer-Aided Pathology: An Available Dataset for Imaging Analysis. *Animals*. 2023;13(9):1563. DOI: [10.3390/ani13091563](https://doi.org/10.3390/ani13091563); PMID: [PMC10177203](https://pubmed.ncbi.nlm.nih.gov/37174600/); PMID: 37174600
7. Martin B, Banner BM, Schäfer EM, Mayr P, Anthuber M, Schenkirsch G, et al. Tumor proportion in colon cancer: results from a semiautomatic image analysis approach. *Virchows Arch*. 2020;477(2):185–93. DOI: [10.1007/s00428-020-02764-1](https://doi.org/10.1007/s00428-020-02764-1); PMID: [PMC7985049](https://pubmed.ncbi.nlm.nih.gov/32076815/); PMID: 32076815
8. Wang KS, Yu G, Xu C, Meng XH, Zhou J, Zheng C, et al. Accurate diagnosis of colorectal cancer based on histopathology images using artificial intelligence. *BMC Med*. 2021;19(1):76. DOI: [10.1186/s12916-021-01942-5](https://doi.org/10.1186/s12916-021-01942-5); PMID: [PMC7986569](https://pubmed.ncbi.nlm.nih.gov/33752648/); PMID: 33752648
9. Bao J, Walliander M, Kovács F, Nagaraj AS, Hemmes A, Sarhadi VK, et al. Spa-RQ: an Image Analysis Tool to Visualise and Quantify Spatial Phenotypes Applied to Non-Small Cell Lung Cancer. *Sci Rep*. 2019;9(1):17613. DOI: [10.1038/s41598-019-54038-9](https://doi.org/10.1038/s41598-019-54038-9); PMID: [PMC6879493](https://pubmed.ncbi.nlm.nih.gov/31772293/); PMID: 31772293
10. Nagpal K, Foote D, Tan F, Liu Y, Chen PHC, Steiner DF, Manoj N, et al. Development and Validation of a Deep Learning Algorithm for Gleason Grading of Prostate Cancer from Biopsy Specimens. *JAMA Oncol*. 2020;6(9):1372–80. DOI: [10.1001/jamaoncol.2020.2485](https://doi.org/10.1001/jamaoncol.2020.2485); PMID: [PMC7378872](https://pubmed.ncbi.nlm.nih.gov/32701148/); PMID: 32701148
11. Kuiava VA, Kuiava EL, Chielle EO, Bittencourt FM De. Artificial intelligence algorithm for the histopathological diagnosis of skin cancer. *Clin Biomed Res*. 2020;40(4):218–22.

12. Li T, Xie P, Liu J, Chen M, Zhao S, Kang W, et al. Automated Diagnosis and Localization of Melanoma from Skin Histopathology Slides Using Deep Learning: A Multicenter Study. *J Healthc Eng.* 2021;2021:5972962. DOI: [10.1155/2021/5972962](https://doi.org/10.1155/2021/5972962); PMCID: [PMC8564171](https://pubmed.ncbi.nlm.nih.gov/34745503/); PMID: [34745503](https://pubmed.ncbi.nlm.nih.gov/34745503/)
13. Raafat KM, El-Zahaby SA. Niosomes of active *Fumaria officinalis* phytochemicals: Antidiabetic, antineuropathic, anti-inflammatory, and possible mechanisms of action. *Chinese Med.* 2020;15:40. DOI: [10.1186/s13020-020-00321-1](https://doi.org/10.1186/s13020-020-00321-1); PMCID: [PMC7195756](https://pubmed.ncbi.nlm.nih.gov/32377229/); PMID: [32377229](https://pubmed.ncbi.nlm.nih.gov/32377229/)
14. Shinouchi R, Shibata K, Hashimoto T, Jono S, Hasumi K, Nobe K. SMTP-44D improves diabetic neuropathy symptoms in mice through its antioxidant and anti-inflammatory activities. *Pharmacol Res Perspect.* 2020;8(6):e00648. DOI: [10.1002/prp2.648](https://doi.org/10.1002/prp2.648); PMCID: [PMC7677968](https://pubmed.ncbi.nlm.nih.gov/33215875/); PMID: [33215875](https://pubmed.ncbi.nlm.nih.gov/33215875/)
15. Sameni H, Panahi M. The Effect of Co-administration of 4-Methylcatechol and Progesterone on Sciatic Nerve Function and Neurohistological Alterations in Streptozotocin-Induced Diabetic Neuropathy in Rats. *Cell J.* 2011;13(1):31-8. PMCID: [PMC3652538](https://pubmed.ncbi.nlm.nih.gov/23671825/); PMID: [23671825](https://pubmed.ncbi.nlm.nih.gov/23671825/)
16. Moscalu M, Moscalu R, Dascălu CG, Țarcă V, Cojocaru E, Costin IM, et al. Histopathological Images Analysis and Predictive Modeling Implemented in Digital Pathology-Current Affairs and Perspectives. *Diagnostics.* 2023;13(14):2379. DOI: [10.3390/diagnostics13142379](https://doi.org/10.3390/diagnostics13142379); PMCID: [PMC10378281](https://pubmed.ncbi.nlm.nih.gov/37510122/); PMID: [37510122](https://pubmed.ncbi.nlm.nih.gov/37510122/)
17. Khan A, Shal B, Khan AU, Ullah R, Baig MW, Ul Haq I, et al. Suppression of TRPV1/TRPM8/P2Y Nociceptors by Withametin via Downregulating MAPK Signaling in Mouse Model of Vincristine-Induced Neuropathic Pain. *Int J Mol Sci.* 2021;22(11):6084. DOI: [10.3390/ijms22116084](https://doi.org/10.3390/ijms22116084); PMCID: [PMC8200233](https://pubmed.ncbi.nlm.nih.gov/34199936/); PMID: [34199936](https://pubmed.ncbi.nlm.nih.gov/34199936/)
18. Labno C. Two Ways to Count Cells with ImageJ. Chicago (IL): Integrated Light Microscopy Core University of Chicago; 2014. p. 1-5. Available from: https://cpb-us-w2.wpmucdn.com/voices.uchicago.edu/dist/c/2275/files/2020/01/cell_counting_automated_and_manual.pdf
19. Lutnick B, Ramon AJ, Ginley B, Csiszer C, Kim A, Flament I, et al. Accelerating pharmaceutical R&D with a user-friendly AI system for histopathology image analysis. *J Pathol Inform.* 2023;14:100337. DOI: [10.1016/j.jpi.2023.100337](https://doi.org/10.1016/j.jpi.2023.100337); PMCID: [PMC10582575](https://pubmed.ncbi.nlm.nih.gov/37860714/); PMID: [37860714](https://pubmed.ncbi.nlm.nih.gov/37860714/)
20. Veta M, Pluim JPW, van Diest PJ, Viergever MA. Breast cancer histopathology image analysis: A review. *IEEE Trans Biomed Eng.* 2014;61(5):1400-11. DOI: [10.1109/tbme.2014.2303852](https://doi.org/10.1109/tbme.2014.2303852); PMID: [24759275](https://pubmed.ncbi.nlm.nih.gov/24759275/)
21. Raghavan V, Rao KR. An ImageJ Based Semi-Automated Morphometric Assessment of Nuclei in Oncopathology. *Int J Sci Study.* 2015;3(7):189-94. DOI: [10.17354/ijss/2015/475](https://doi.org/10.17354/ijss/2015/475)
22. Aeffner F, Zarella MD, Buchbinder N, Bui MM, Goodman MR, Hartman DJ, et al. Introduction to Digital Image Analysis in Whole-slide Imaging: A White Paper from the Digital Pathology Association. *J Pathol Inform.* 2019;10:9. DOI: [10.4103/jpi.jpi_82_18](https://doi.org/10.4103/jpi.jpi_82_18); PMCID: [PMC6437786](https://pubmed.ncbi.nlm.nih.gov/30984469/); PMID: [30984469](https://pubmed.ncbi.nlm.nih.gov/30984469/)
23. Herbert A. Single Molecule Light Microscopy ImageJ Plugins. East Sussex (UK): University of Sussex; 2014. p. 1-156. Available from: <http://www.sussex.ac.uk/gdsc/intranet/pdfs/SMLM.pdf>
24. Anggraeni DT. Perbaikan Citra Dokumen Hasil Pindai Menggunakan Metode Simple, Adaptive-Gaussian, dan Otsu Binarization Thresholding. *EXPERT J Manajemen Sistem Informasi Teknologi.* 2021;11(2):71-7. DOI: [10.36448/expert.v11i2.2170](https://doi.org/10.36448/expert.v11i2.2170)
25. Korzynska A, Roszkowiak L, Lopez C, Bosch R, Witkowski L, Lejeune M. Validation of various adaptive threshold methods of segmentation applied to follicular lymphoma digital images stained with 3,3'-Diaminobenzidine&Haematoxylin. *Diagn Pathol.* 2013;8:48. DOI: [10.1186/1746-1596-8-48](https://doi.org/10.1186/1746-1596-8-48); PMCID: [PMC3656801](https://pubmed.ncbi.nlm.nih.gov/23531405/); PMID: [23531405](https://pubmed.ncbi.nlm.nih.gov/23531405/)
26. Rehman NA, Haroon F. Adaptive Gaussian and Double Thresholding for Contour Detection and Character Recognition of Two-Dimensional Area Using Computer Vision. *Eng Proc.* 2023;32(1):23. DOI: [10.3390/engproc2023032023](https://doi.org/10.3390/engproc2023032023)

27. Kowal M, Filipczuk P, Obuchowicz A, Korbicz J. Computer-aided diagnosis of breast cancer based on fine needle biopsy microscopic images. *Comput Biol Med.* 2013;43(10):1563–72. DOI: [10.1016/j.combiomed.2013.08.003](https://doi.org/10.1016/j.combiomed.2013.08.003); PMID: [24034748](https://pubmed.ncbi.nlm.nih.gov/24034748/)
28. Das A, Nair MS, Peter SD. Computer-Aided Histopathological Image Analysis Techniques for Automated Nuclear Atypia Scoring of Breast Cancer: a Review. *J Digit Imaging.* 2020;33(5):1091–121. DOI: [10.1007/s10278-019-00295-z](https://doi.org/10.1007/s10278-019-00295-z); PMCID: [PMC7573034](https://pubmed.ncbi.nlm.nih.gov/31989390/); PMID: [31989390](https://pubmed.ncbi.nlm.nih.gov/31989390/)
29. Suarez-Arnedo A, Figueroa FT, Clavijo C, Arbeláez P, Cruz JC, Muñoz-Camargo C. An image J plugin for the high throughput image analysis of in vitro scratch wound healing assays. *PLoS One.* 2020;15(7):e0232565. DOI: [10.1371/journal.pone.0232565](https://doi.org/10.1371/journal.pone.0232565); PMCID: [PMC7386569](https://pubmed.ncbi.nlm.nih.gov/32722676/); PMID: [32722676](https://pubmed.ncbi.nlm.nih.gov/32722676/)
30. Chan HP, Hadjiiski LM, Samala RK. Computer-aided diagnosis in the era of deep learning. *Med Phys.* 2020;47(5):e218-27. DOI: [10.1002/mp.13764](https://doi.org/10.1002/mp.13764); PMCID: [PMC7293164](https://pubmed.ncbi.nlm.nih.gov/32418340/); PMID: [32418340](https://pubmed.ncbi.nlm.nih.gov/32418340/)
31. Brixtel R, Bougleux S, Lézoray O, Caillot Y, Lemoine B, Fontaine M, et al. Whole Slide Image Quality in Digital Pathology: Review and Perspectives. *IEEE Access.* 2022;10:131005-35. DOI: [10.1109/ACCESS.2022.3227437](https://doi.org/10.1109/ACCESS.2022.3227437)